

A broadband controller for shunt piezoelectric damping of structural vibration

S Behrens¹, A J Fleming and S O R Moheimani

School of Electrical Engineering and Computer Science, University of Newcastle,
NSW 2304, Australia

E-mail: sbehrens@ecemail.newcastle.edu.au

Received 22 May 2001, in final form 20 August 2002

Published 10 January 2003

Online at stacks.iop.org/SMS/12/18

Abstract

In this paper a broadband active shunt technique for controlling vibration in piezoelectric laminated structures is proposed. The effect of the negative capacitance controller is studied theoretically and then validated experimentally on a piezoelectric laminated simply supported plate. The ‘negative capacitance controller’ is similar in nature to passive shunt damping techniques, as a single piezoelectric transducer is used to dampen multiple modes. While achieving comparable performance to that of the passive shunt schemes, the negative capacitance controller has a number of advantages. It is simpler to implement, less sensitive to environmental variations and can be considered as a broadband vibration absorber.

1. Introduction

Placing an electrical impedance across the terminals of a piezoelectric transducer, which is normally bonded to or embedded in the flexible mechanical structure with a view to minimizing structural vibrations, is referred to as piezoelectric shunt damping. As the piezoelectric laminated structure strains, an electrical charge forms on the terminals of the transducer. By designing an appropriate electrical impedance across the terminals of the transducer, the circuit network is capable of increasing the mechanical damping of the host structure.

A passive shunt damper [4, 9, 10, 16, 17] consists of an impedance network made from *passive* elements e.g. capacitors, inductors and resistors. Most passive schemes act to minimize structural vibration at a particular frequency associated with a lightly damped structural vibration mode. These frequencies are rarely stationary in real applications, e.g. changes in climatic conditions may shift resonance frequencies of the structure. Some damping is usually added to ensure effectiveness over a range of frequencies. Therefore, maximum amplitude reduction is achieved only if the shunt absorber is lightly damped and precisely tuned to the required frequency of concern.

The concept of negative capacitor shunts for vibration control of piezoelectric laminates was first introduced by Forward [8] who suggested that a negative capacitor in parallel with a resistor, shunted across a piezoelectric transducer, could be used to reduce structural vibration. More recent work on this topic includes [2, 18, 19].

The purpose of this paper is two-fold: it seeks to present a thorough analysis of the operation of negative capacitor shunts, and it proposes an effective implementation of the said system. The ‘negative capacitance controller’ is studied theoretically and then validated experimentally on a piezoelectric laminated structure. It is similar in nature to passive shunt damping techniques as a single piezoelectric transducer is used, capable of damping multiple modes, less sensitive to environmental conditions, considerably robust and capable of damping modally dense structures, i.e. broadband.

The paper is organized as follows. Section 2 will introduce the piezoelectric effect and how to model a piezoelectric transducer. In section 3, a model is developed of a piezoelectric laminated plate structure, while in section 4, we notice that the piezoelectric shunted composite system is in fact a feedback control problem. The next section, section 5, presents the proposed active shunt ‘negative capacitance controller’. Section 6 reports simulated and experimental results that verify the proposed control scheme. For section 7, we address the

¹ Author to whom any correspondence should be addressed.

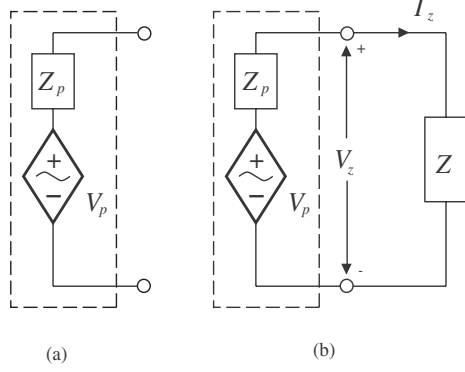


Figure 1. (a) Series equivalent model for piezoelectric transducer, and (b) schematic of piezoelectric shunting layer with a shunting impedance Z present.

stability and robustness of the closed loop composite system. Finally in section 8, the paper is concluded.

2. Piezoelectric model

The piezoelectric effect was first discovered in 1880 by Pierre and Jacques Curie, who demonstrated that, when certain crystals were stressed, an electrical charge was produced on the material surface. It was subsequently demonstrated that the converse effect was true. That is, when an electrical field was applied to a piezoelectric material it changed its shape and size. The piezoelectric effect has been observed in a number of natural materials such as quartz crystals and Rochelle salt. However, it can be artificially manufactured, such as barium titanate, polyvinylfluoride (PVDF) and lead zirconate titanate (PZT). The last two materials are commonly used for vibration control.

For vibration control, a thin sliver of piezoelectric material is sandwiched between two conducting layers. This forms a piezoelectric transducer. The transducer is then glued to the surface of the flexible structure using a strong adhesive material. Sometimes the piezoelectric transducer is laminated within the flexible structure.

Piezoelectric transducers behave electrically like a series capacitor–resistor and mechanically like a stiff spring [5]. It is common to model the piezoelectric element as a series capacitor C_p , resistor R_p and a strain-dependent voltage source V_p . This is shown in figure 1(a), where for generality the internal impedance is considered to be $Z_p(s)$. Naturally, $Z(s) = \frac{1}{C_p s} + R_p$. However, more complex forms of the internal impedance can be allowed. The internal dielectric resistance R_p is typically within the range 50–100 Ω and is sometime neglected.

3. Dynamics of a piezoelectric laminate plate

To facilitate in the development of the proposed negative capacitance controller, a mathematical model is developed for a thin flexible plate structure. A popular method for modelling piezoelectric laminate structures is *modal analysis* [13]. Using the modal analysis procedure, the plate transverse deflection at a point with respect to time position function $w(x, y, t)$ can be

modelled. This function can be expanded as an infinite series, as

$$w(x, y, t) = \sum_{m=1}^{\infty} \sum_{n=1}^{\infty} W_{mn}(x, y) q_{mn}(t), \quad (1)$$

where $(x, y) \in \mathcal{R}$, $\mathcal{R} = \{(x, y) | 0 \leq x \leq L_x, 0 \leq y \leq L_y\}$, $q_{mn}(t)$ is referred to as the modal displacement or generalized coordinate and $W_{mn}(x, y)$ is the plate displacement modal amplitude. The mode numbers in the directions of x and y are represented by m and n , i.e. for our case $(m, n) = (1, 1), (2, 1), (1, 2), (3, 1), (2, 2), (3, 2), \dots$

Consider a thin plate with dimensions of $L_x \times L_y \times h$ as shown in figure 2. Piezoelectric actuating and shunting layers of dimensions $L_{px} \times L_{py} \times h_p$ are bonded to the surface of the plate on both sides. The partial differential equation that governs the dynamics of the thin plate is [7, 13]

$$D \left(\frac{\partial^4 w(x, y, t)}{\partial x^4} + 2 \frac{\partial^4 w(x, y, t)}{\partial x^2 \partial y^2} + \frac{\partial^4 w(x, y, t)}{\partial y^4} \right) + \rho \ddot{w} = \frac{\partial^2 M_{px}}{\partial x^2} + \frac{\partial^2 M_{py}}{\partial y^2}, \quad (2)$$

where the term $D = \frac{Eh^3}{12(1-\nu^2)}$ is the flexural rigidity of the plate, and M_{px} and M_{py} are defined as the moments generated by the piezoelectric actuating layer per unit length along x and y directions. For the plate, ρ represents the mass per unit area, h is the thickness, while E and ν are the Young's modulus and the Poisson's ratio, respectively.

For a simply supported plate the following boundary conditions hold:

$$\begin{aligned} w(0, y, t) &= w(L_x, y, t) = 0 \\ w(x, 0, t) &= w(x, L_y, t) = 0 \\ \frac{\partial^2 w(0, y, t)}{\partial x^2} &= \frac{\partial^2 w(L_x, y, t)}{\partial x^2} = 0 \\ \frac{\partial^2 w(x, 0, t)}{\partial y^2} &= \frac{\partial^2 w(x, L_y, t)}{\partial y^2} = 0. \end{aligned} \quad (3)$$

The eigenfunction that satisfies these boundary conditions and the eigenvalue problem can be shown to be a double-sinusoidal function [7], as

$$W_{mn}(x, y) = \frac{2}{\sqrt{L_x L_y}} \sin\left(\frac{m\pi x}{L_x}\right) \sin\left(\frac{n\pi y}{L_y}\right), \quad (4)$$

while the natural frequencies ω_{mn} of the thin plate with the above boundary conditions satisfy [7]

$$\omega_{mn} = \sqrt{\frac{D}{\rho}} \left[\left(\frac{m\pi}{L_x}\right)^2 + \left(\frac{n\pi}{L_y}\right)^2 \right]. \quad (5)$$

A common arrangement for the piezoelectric elements is the two-dimensional antisymmetric *wafer* configuration [7]. This configuration assumes that the piezoelectric elements are larger in the x and y directions compared to the z direction, i.e. $L_{px}, L_{py} \gg h_p$. Since the piezoelectric layers are symmetrical when a voltage is applied across the electrodes of the actuating element, it induces equal surface strains to the plate in the x and y directions, i.e. $M_{px} = M_{py}$.

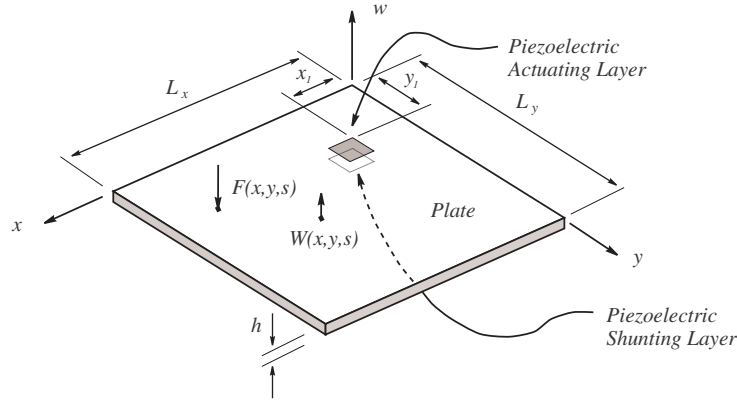


Figure 2. A thin simply supported plate with actuating and shunting piezoelectric layers attached.

From the modal analysis solution, the transfer function from the applied disturbance voltage $V_a(s)$ to the plate deflection $W(x, y, s)$ can be written as

$$G_{wv}(s) \triangleq \frac{W(x, y, s)}{V_a(s)} = \frac{C_a}{\rho} \sum_{m=1}^{\infty} \sum_{n=1}^{\infty} \frac{W_{mn}(x, y) \phi_{mn}}{s^2 + 2\zeta_{mn}\omega_{mn}s + \omega_{mn}^2}, \quad (6)$$

where ζ_{mn} is the damping coefficient, which is normally determined experimentally. C_a is based on the properties of the plate and the piezoelectric actuating layer:

$$C_a = DK^f \frac{d_{31}}{h_p} \quad (7)$$

where d_{31} is the strain constant and h_p is the thickness of the piezoelectric layer. K^f is a geometric constant which depends on the properties of the actuating layer and the plate [7]:

$$K^f = \frac{12E_p h_p (h_p + h)(1 + \nu)}{E_p((h + 2h_p)^3 - h^3) + 24D(1 + \nu)(1 - \nu_p)}. \quad (8)$$

Here, E_p and ν_p are the Young's modulus and the Poisson's ratio of the piezoelectric layer. Furthermore, the function term ϕ_{mn} depends on the location of the actuator layer on the plate surface, such that [11]

$$\begin{aligned} \phi_{mn} = & 2 \frac{mL_y^{1/2}}{nL_x^{3/2}} \left[\cos\left(\frac{n\pi y_1}{L_y}\right) - \cos\left(\frac{n\pi y_2}{L_y}\right) \right] \\ & \times \left[\cos\left(\frac{m\pi x_2}{L_x}\right) - \cos\left(\frac{m\pi x_1}{L_x}\right) \right] \\ & + 2 \frac{nL_x^{1/2}}{mL_y^{3/2}} \left[\cos\left(\frac{m\pi x_1}{L_x}\right) - \cos\left(\frac{m\pi x_2}{L_x}\right) \right] \\ & \times \left[\cos\left(\frac{n\pi y_2}{L_y}\right) - \cos\left(\frac{n\pi y_1}{L_y}\right) \right]. \end{aligned} \quad (9)$$

Note that (x_1, x_2) and (y_1, y_2) are the coordinates of a corner of the actuating layer, as shown in figure 2, such that $x_2 = x_1 + L_{px}$ and $y_2 = y_1 + L_{py}$.

The transfer function between the applied voltage $V_a(s)$ and the shunting layer output voltage $V_s(s)$, can also be found as

$$G_{vv}(s) \triangleq \frac{V_s(s)}{V_a(s)} = \frac{C_s C_a}{\rho} \sum_{m=1}^{\infty} \sum_{n=1}^{\infty} \frac{B_{mn} \phi_{mn}}{s^2 + 2\zeta_{mn}\omega_{mn}s + \omega_{mn}^2}, \quad (10)$$

where [11]

$$\begin{aligned} B_{mn} = & \frac{\sqrt{L_x L_y}}{mn} \left[\left(\frac{m}{L_x}\right)^2 + \left(\frac{n}{L_y}\right)^2 \right] \\ & \times \left[\cos\left(\frac{m\pi x_1}{L_x}\right) - \cos\left(\frac{m\pi x_2}{L_x}\right) \right] \\ & \times \left[\cos\left(\frac{n\pi y_1}{L_y}\right) - \cos\left(\frac{n\pi y_2}{L_y}\right) \right]. \end{aligned} \quad (11)$$

Using the same assumptions as the actuating layer, the shunting layer geometric constant C_s can be determined as

$$C_s = -\left(\frac{h}{2} + h_p\right) \left(\frac{k_{31}^2}{g_{31} C_p}\right), \quad (12)$$

where k_{31} is the electromechanical coupling factor, g_{31} is the stress voltage coefficient, and C_p is the capacitance of the shunting piezoelectric layer.

With reference to figure 2, we can also derive the following two transfer functions if a point force disturbance $F(x, y, s)$ is applied to the plate structure, as [1, 2]

$$G_{vf}(s) \triangleq \frac{V_s(s)}{F(x, y, s)} = \sum_{m=1}^{\infty} \sum_{n=1}^{\infty} \frac{B_{mn} F_{mn}(x, y)}{s^2 + 2\zeta_{mn}\omega_{mn}s + \omega_{mn}^2}, \quad (13)$$

and

$$G_{wf}(s) \triangleq \frac{W(x, y, s)}{F(x, y, s)} = \sum_{m=1}^{\infty} \sum_{n=1}^{\infty} \frac{W_{mn}(x, y) F_{mn}(x, y)}{s^2 + 2\zeta_{mn}\omega_{mn}s + \omega_{mn}^2}. \quad (14)$$

When designing shunt impedance, we may be interested only in a particular bandwidth. For obvious reasons, the infinite-order models produced by the modal analysis technique may not be suitable. Thus, an alternative method has been introduced in [3] where G_{wv} and G_{vv} have a low pass roll-off term. Therefore, we have the following modified transfer functions:

$$\begin{aligned} G_{wv}(s) \triangleq \frac{W(x, y, s)}{V_a(s)} = & \frac{C_a}{\rho} \sum_{m=1}^M \sum_{n=1}^N \frac{W_{mn}(x, y) \phi_{mn}}{s^2 + 2\zeta_{mn}\omega_{mn}s + \omega_{mn}^2} \\ & + \frac{K_{opt}^w \omega_c^2}{s^2 + 2\zeta_c \omega_c s + \omega_c^2}, \end{aligned} \quad (15)$$

$$G_{vv}(s) \triangleq \frac{V_s(s)}{V_a(s)} = \frac{C_s C_a}{\rho} \sum_{m=1}^M \sum_{n=1}^N \frac{B_{mn} \phi_{mn}}{s^2 + 2\zeta_{mn} \omega_{mn} s + \omega_{mn}^2} + \frac{K_{opt}^v \omega_c^2}{s^2 + 2\zeta_c \omega_c s + \omega_c^2}, \quad (16)$$

where ζ_c was assumed to be some damping and the cut-off frequency ω_c was chosen to $\omega_c \gg \max(\omega_{mn})$. The DC feedthrough terms K_{opt}^w and K_{opt}^v are the zero-frequency correction terms introduced in [3, 14, 15].

4. Modelling the composite system

Consider figure 1(b), where a piezoelectric patch is shunted by an impedance $Z(s)$. Hence, the current–voltage relationship corresponding to the impedance can be represented as

$$V_z(s) = I_z(s)Z(s), \quad (17)$$

where $V_z(s)$ is the voltage across the impedance, and $I_z(s)$ is the current flowing through the impedance $Z(s)$. Applying Kirchhoff's voltage law to the circuit shown in figure 1(b), we obtain the following relationship for $V_z(s)$, in terms of $V_p(s)$ and $I_z(s)$:

$$V_z(s) = V_p(s) - Z_p(s)I_z(s), \quad (18)$$

where $V_p(s)$ is the voltage induced from the electromechanical coupling effect [9] and $Z_p(s)$ is the internal impedance of the piezoelectric element. For an ‘ideal’ piezoelectric transducer, $Z_p(s) = \frac{1}{C_p s}$. However, to account for the dielectric losses we may add a resistive term to $Z_p(s)$, i.e. $Z_p(s) = \frac{1}{C_p s} + R_p$. Using (17) and (18), we obtain

$$V_z(s) = \frac{Z(s)}{Z(s) + Z_p(s)} V_p(s). \quad (19)$$

Now, assume that the structure is disturbed by a voltage $V_{in}(s)$, which is applied to the actuating layer and some impedance is attached to the piezoelectric terminals, then the overall linear relationship is [1, 2]

$$V_p(s) = G_{vv}(s)V_{in}(s) - G_{vv}(s)V_z(s), \quad (20)$$

where $G_{vv}(s)$ is the open loop transfer function from $V_s(s)$ to $V_a(s)$. Note that $V_s(s)$ is dynamically equivalent to $V_p(s)$ when no load is applied across the terminals of the shunting piezoelectric layer, i.e. $V_p(s) = G_{vv}(s)V_{in}(s)$ for $Z(s) = \infty$.

By substituting (19) into the above equation, $V_p(s)$ is found to be

$$V_p(s) = G_{vv}(s)V_{in}(s) - G_{vv}(s) \frac{Z(s)}{Z(s) + Z_p(s)} V_p(s).$$

Using simple algebra, the closed loop transfer function relating $V_p(s)$ to $V_{in}(s)$ can be found as [1, 2]

$$\hat{G}_{vv}(s) \triangleq \frac{V_p(s)}{V_{in}(s)} = \frac{G_{vv}(s)}{1 + G_{vv}(s)K(s)}, \quad (21)$$

where the effective controller $K(s)$ is

$$K(s) = \frac{Z(s)}{Z(s) + Z_p(s)}. \quad (22)$$

Note that the following relationship can also be derived for the displacement at a given location $W(x, y, s)$ to $V_{in}(s)$ [1, 2]:

$$\hat{G}_{vw}(s) \triangleq \frac{W(x, y, s)}{V_{in}(s)} = \frac{G_{vw}(s)}{1 + G_{vv}(s)K(s)}. \quad (23)$$

From equations (21)–(23) it can be observed that shunt damping of a piezoelectric transducer is indeed a feedback control problem. Therefore, it should be possible to use feedback control techniques to determine an appropriate shunting impedance.

Aside, assuming $Z(s) = \infty$, we can define the following transfer functions, as

$$G_{vf}(s) \triangleq \left. \frac{V_s(s)}{F(x, y, s)} \right|_{V_{in}(s)=0}$$

$$G_{wf}(s) \triangleq \left. \frac{W(x, y, s)}{F(x, y, s)} \right|_{V_{in}(s)=0}$$

$$G_{vv}(s) \triangleq \left. \frac{V_s(s)}{V_a(s)} \right|_{F(x, y, s)=0}$$

$$G_{vw}(s) \triangleq \left. \frac{W(x, y, s)}{V_a(s)} \right|_{F(x, y, s)=0}.$$

If the host structure is disturbed simultaneously by a point force $F(x, y, s)$ and a voltage $V_{in}(s)$, assuming $Z(s) = \infty$, we may write

$$V_p(s) = G_{vf}(s)F(x, y, s) + G_{vv}(s)V_{in}(s). \quad (24)$$

Now, assuming the piezoelectric patch is shunted by some impedance $Z(s)$, the above expression for $V_p(s)$ becomes

$$V_p(s) = G_{vf}(s)F(x, y, s) - G_{vv}(s)K(s)V_p(s) + G_{vv}(s)V_{in}(s). \quad (25)$$

Therefore, the voltage in terms of $V_p(s)$ is

$$V_p(s) = \frac{G_{vf}(s)}{1 + K(s)G_{vv}} F(x, y, s) + \frac{G_{vv}(s)}{1 + K(s)G_{vv}} V_{in}(s), \quad (26)$$

and the displacement $W(x, y, s)$ is

$$W(x, y, s) = \frac{G_{wf}(s)}{1 + K(s)G_{vv}(s)} F(x, y, s) + \frac{G_{vw}(s)}{1 + K(s)G_{vv}(s)} V_{in}(s) \quad (27)$$

where $G_{wf}(s) \triangleq G_{vf}(s)G_{vw}(s)$. A summary of the system block diagrams for both equations (26) and (27) is shown in figure 3.

5. Developing the negative capacitance controller

In this section we develop a class of high-performance broadband shunt controllers for vibration control of piezoelectric laminates. Consider the closed loop transfer function $\hat{G}_{vv}(s)$, from equation (21), as

$$\hat{G}_{vv}(s) = \frac{G_{vv}(s)}{1 + G_{vv}(s)K(s)}, \quad (28)$$

with the effective controller

$$K(s) = \frac{Z(s)}{Z(s) + Z_p(s)}, \quad (29)$$

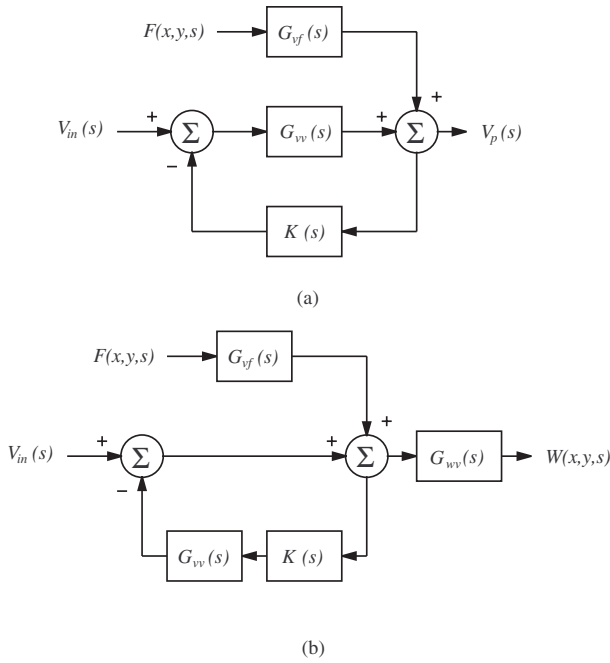


Figure 3. Composite system transfer function block diagram: (a) represents equation (26) and (b) represents equation (27).

where $Z_p(s) = \frac{1}{C_p s} + R_p$. Note that the dielectric resistance R_p has been added for the sake of completeness. After straightforward manipulations, we obtain the following modified expression for $\hat{G}_{vv}(s)$, as

$$\hat{G}_{vv}(s) = \frac{G_{vv}(s)[Z(s) + Z_p(s)]}{Z(s) + Z_p(s) + Z(s)G_{vv}(s)}. \quad (30)$$

The modified closed loop transfer function (30) can be reduced to zero by selecting the optimal shunt impedance $Z_{opt}(s) = -Z_p(s)$. That is, $Z_{opt}(s) = -\frac{1}{C_p s} - R_p$. It should be noted that $Z_{opt}(s)$ is not a realizable network as it creates an undamped electrical resonance, or alternatively, requires that the shunted piezoelectric transducer has an infinite stiffness. However, $Z_{opt}(s)$ can be approximated, reasonably closely, within a specific bandwidth. Figure 4 demonstrates an effective way of achieving this objective. The figure shows the proposed ‘negative capacitance controller’ connected to the terminals of the lossless piezoelectric element. Since the dielectric resistance R_p is significantly smaller than the impedance of the capacitor within the frequency range of interest, we can safely assume that $Z_p(s) = \frac{1}{C_p s}$.

If $Z(s)$ is chosen to be $-\frac{1}{C_s} + R$, then $Z(s)$ will have the following impedance transfer function:

$$Z(s) = \frac{RCs - 1}{Cs}. \quad (31)$$

Substituting (31) in (29), the effective controller $K(s)$ becomes

$$K(s) = \frac{s - \frac{1}{RC}}{s + \frac{1}{RC}(\frac{C}{C_p} - 1)}. \quad (32)$$

As we wish to work with a stable controller $K(s)$, we need to ensure that the capacitance C is chosen to be larger than

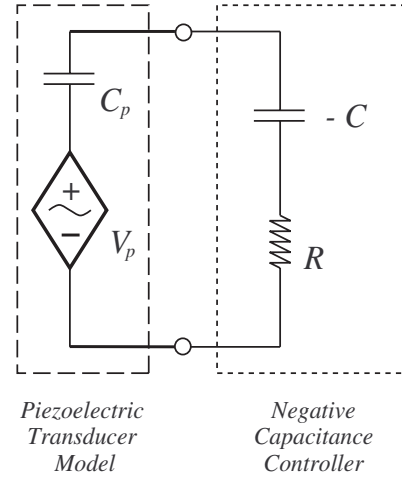


Figure 4. Proposed negative capacitance controller with appropriate damping resistance.

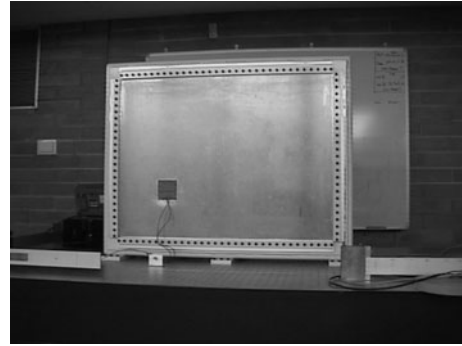


Figure 5. Piezoelectric laminated simply supported plate structure.

the capacitance of the piezoelectric transducer, i.e. $C > C_p$. In practice the equivalent electrical model of the piezoelectric element does not fully describe the piezoelectric dynamics, i.e. the electrical model contains some uncertainty. To deal with this uncertainty, C has to be chosen conservatively.

6. Simulation and experimental verification

6.1. Simply supported plate apparatus

Experiments were carried out at the Laboratory for Dynamics and Control of Smart Structures². A photograph of the piezoelectric laminated plate structure is shown in figure 5. The experimental plate is of uniform thickness and experimentally pinned at all edges. A pair of piezoelectric ceramic patches are attached symmetrically to either side of the plate surface in a collocated manner, as shown in figure 2. One patch is used as the actuating layer and the other as the shunting layer. Dimensions of the plate and physical properties of the piezoelectric layers are summarized in tables 1 and 2, respectively. For a detailed description of the apparatus, the reader is referred to [11].

When observing the dynamics of a structure, it is common practice to consider the transfer function between the displacement at any point on the structure and the actuator

² <http://rumi.newcastle.edu.au/>

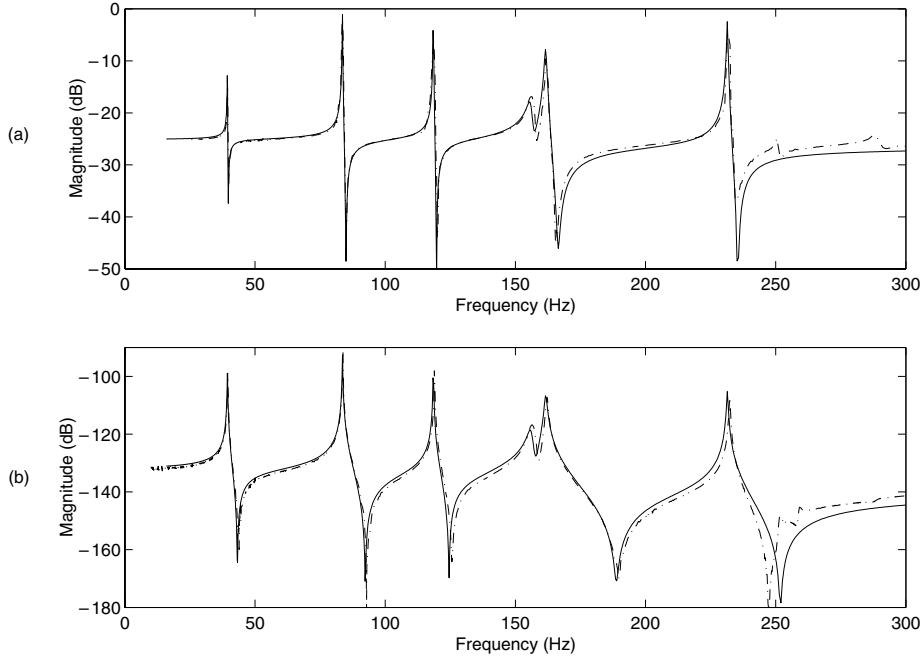


Figure 6. Experimental (— · —) and modelled (—) frequency response of (a) $|G_{vv}(s)|$ and (b) $|G_{wv}(0.2, 0.2, s)|$.

Table 1. Parameters of the simply supported plate.

Name	Symbol	Unit
Length (m)	L_x	0.8
Length (m)	L_y	0.6
Thickness (m)	h	0.004
Young's modulus (10^9 N m^{-2})	E	65
Poisson's ratio	ν	0.3
Mass/unit area (kg m^{-2})	ρ	10.6

disturbance voltage $G_{wv}(s)$. Also, the dynamics between the shunting piezoelectric voltage and the actuator voltage $G_{vv}(s)$.

The displacement and voltage frequency responses, $G_{wv}(s)$ and $G_{vv}(s)$, are measured using a Polytec laser scanning vibrometer (PSV-300) and a Hewlett Packard spectrum analyzer (35670A). In both cases, a swept sine excitation is applied to the actuating piezoelectric layer as a disturbance. The frequency response of the experimental system and identified model are shown in figure 6. It can be observed that the identified model is a good representation of the true system for the first six modes of interest.

6.2. Simulated results

In order to find an appropriate value for resistor R , an optimization approach is proposed [3]. The \mathcal{H}_2 norm of the composite system $\hat{G}_{wv}(s)$ is minimized for the first six structural modes. This requires a solution to the following constrained optimization problem to be found:

$$R^* = \arg \min_{R>0} \|\hat{G}_{wv}(0.2, 0.2, s)\|_2 \quad (33)$$

where $\hat{G}_{wv}(0.2, 0.2, s)$ is the shunt transfer function from the applied disturbance voltage $V_{in}(s)$ to the deflection $W(x, y, s)$ at a point $x = y = 0.2 \text{ m}$ on the plate surface. Note for our case

C was chosen to be 485 nF, since the measured piezoelectric capacitance is $C_p = 471 \text{ nF}$.

Using a line search algorithm, a local minimum was found at $R^* = 80.2 \Omega$. Figure 7 shows the \mathcal{H}_2 norm cost surface which contains a minima at R^* . Since the optimization is performed on a single variable, finding a minimum is generally a straightforward problem and can be done by inspecting figure 7.

Using $C = 485 \text{ nF}$ and $R^* = 80.2 \Omega$, simulations of open loop $G_{wv}(0.2, 0.2, s)$ and closed loop $\hat{G}_{wv}(0.2, 0.2, s)$ show that the structural modes of the plate have been considerably dampened, as shown in figure 8. From figure 9, we can observe that the poles of the compound system have been pushed further to the left. By shifting the poles to the left we have effectively added damping to the mechanical system, and therefore we have minimized the vibration of the structure. From figure 9, we can foresee that the controller has a localized effect on the closed loop poles.

6.3. Implementing a negative capacitance

The main question here is how may a negative capacitance circuit be implemented? To answer this question consider figure 10. The circuit shown is one of a general class of circuits known as a *negative impedance converter* (NIC) [6, 12]. The input impedance $Z_{in}(s)$ is equivalent to

$$Z_{in}(s) = -\frac{R_1}{R_2} Z_L. \quad (34)$$

Thus, if $Z_L = \frac{1}{C_s}$ then $Z_{in}(s) = -\frac{R_1}{R_2} \frac{1}{C_s}$. We can create a negative capacitance, which scales Z_L by the ratios of the resistors R_1 and R_2 , i.e. a transconductance gain.

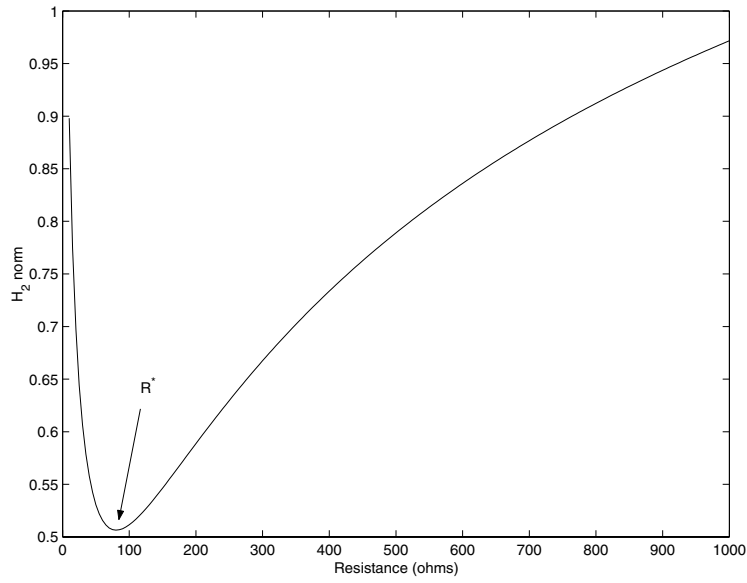


Figure 7. $\|\hat{G}_{wv}(0.2, 0.2, s)\|_2$ versus resistance R (Ω).

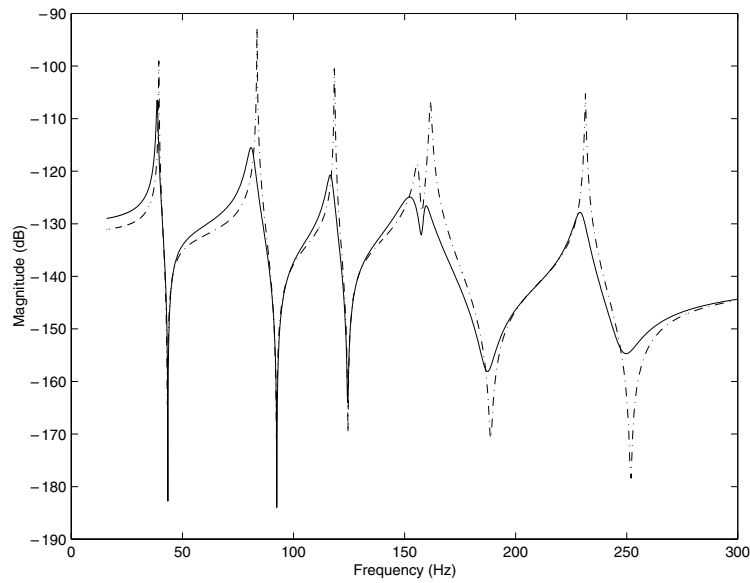


Figure 8. Simulated response: $|G_{wv}(0.2, 0.2, s)|$ system (— · —) and $|\hat{G}_{wv}(0.2, 0.2, s)|$ system (—).

Table 2. Piezoelectric transducer parameters.

Name	Symbol	Unit
Location x direction (m)	x_1	0.1536
Location y direction (m)	y_1	0.1418
Length (m)	$L_{px} L_{py}$	0.0724
Thickness (m)	h_p	0.00191
Capacitance (10^{-9} F)	C_p	471
Young's modulus (10^9 N m $^{-2}$)	E_p	62
Poisson's ratio	ν_p	0.3
Strain constant (10^{-12} m V $^{-1}$)	d_{31}	-320
Electromechanical coupling factor	k_{31}	0.44
Stress constant/voltage coefficient (10^{-3} V m N $^{-1}$)	g_{31}	-9.5

6.4. Experimental verification

The proposed negative capacitance controller, shown in figure 11, was constructed using the appropriate components,

as tabulated in table 3. Construction of the active shunt circuit incorporated a Burr-Brown OPA445 high voltage operational amplifier. Note that an additional resistor \hat{R} was placed in

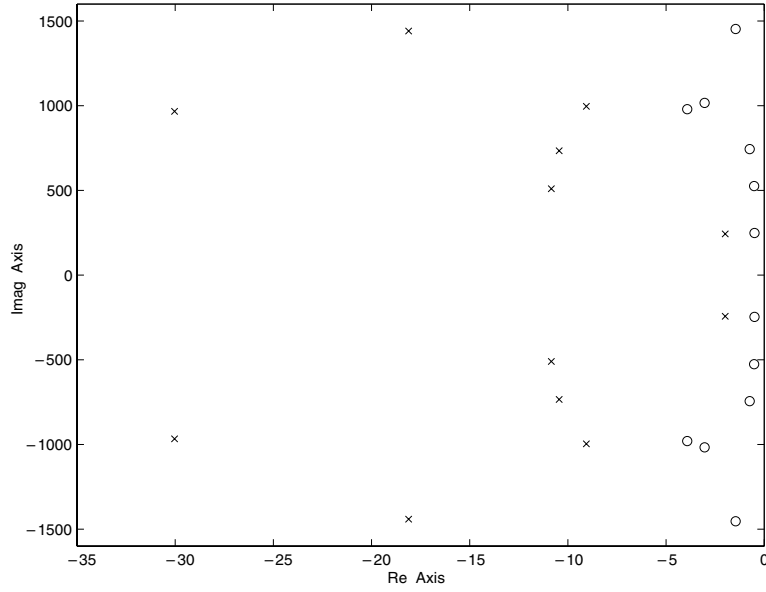


Figure 9. Simulated open loop (o) and closed loop (x) poles of the plate structure.

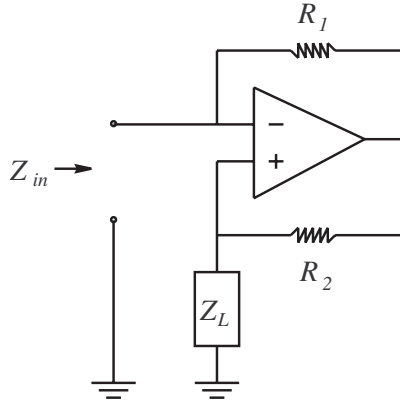


Figure 10. Example of a negative impedance converter.

Table 3. Parameters of negative capacitance circuit.

Circuit component	Value
$R_1 R_2$ (k Ω)	10
\hat{R} (M Ω)	1
C (nF)	485
R (Ω)	80

parallel to the capacitor C to increase the leakage of the capacitor. This is undesirable, but necessary, due to the bias currents flowing from the non-ideal operational amplifier. The parallel resistor and capacitor effectively acts like a high pass filter allowing bias currents to flow to ground, thus preventing the capacitor from acquiring a DC charge.

Now, the experimental negative impedance is $Z_{in}(s) = -\frac{R_1}{R_2} \frac{\hat{R}}{RCs+1}$ and if we assume that $R_1 = R_2$ the experimental impedance $\tilde{Z}(s)$ can be written as

$$\tilde{Z}(s) = \frac{Rs + \frac{1}{C} \left(\frac{R}{\hat{R}} - 1 \right)}{s + \frac{1}{RC}}. \quad (35)$$

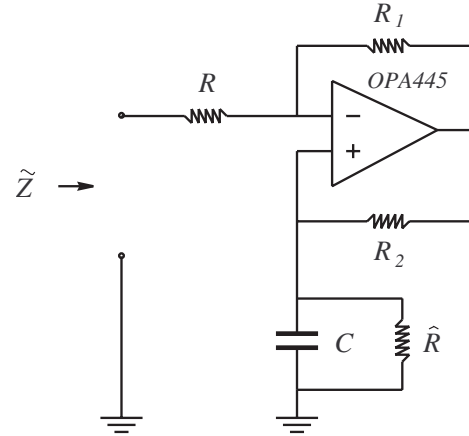


Figure 11. Experimental negative capacitance controller.

Therefore, the effective controller $\tilde{K}(s)$ is

$$\tilde{K}(s) = \frac{s^2 + \frac{(R-\hat{R})}{R\hat{R}C}s}{s^2 + \frac{RC_p + \hat{R}(C-C_p)}{R\hat{R}CC_p}s + \frac{1}{R\hat{R}CC_p}}. \quad (36)$$

Both equations (35) and (36) are stable, if $C > C_p$ and $\hat{R} \gg R > 0$.

Using the described circuit, shown in figure 11, the active shunting is now applied to the piezoelectric laminated simply supported plate. A swept sine voltage was applied to the actuator layer as a disturbance and the closed loop frequency response, $\hat{G}_{wv}(0.2, 0.2, s)$, was obtained using the Polytec laser scanning vibrometer (PSV-300).

Figure 12 compares the open loop $|G_{wv}(0.2, 0.2, s)|$ and closed loop $|\hat{G}_{wv}(0.2, 0.2, s)|$ responses. Experimental resonant amplitudes for the first to sixth modes were successfully reduced by 5.8, 20.1, 18.2, 3.8, 16.7 and 17.2 dB. From theoretical simulations, resonant amplitudes were expected to decrease by 6.8, 22.8, 20.1, 6.2, 19.6

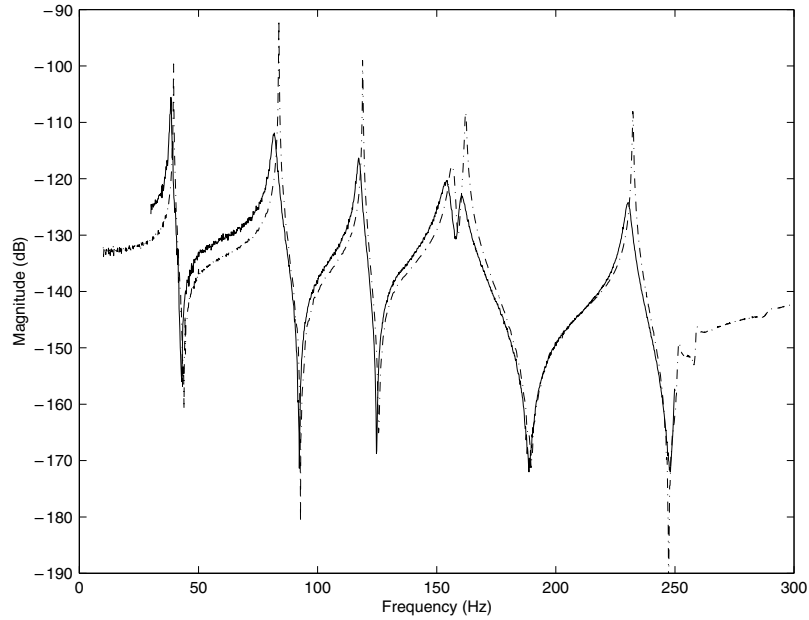


Figure 12. Experimental response: $|G_{wv}(0.2, 0.2, s)|$ system (---) and $|\hat{G}_{wv}(0.2, 0.2, s)|$ system (—).

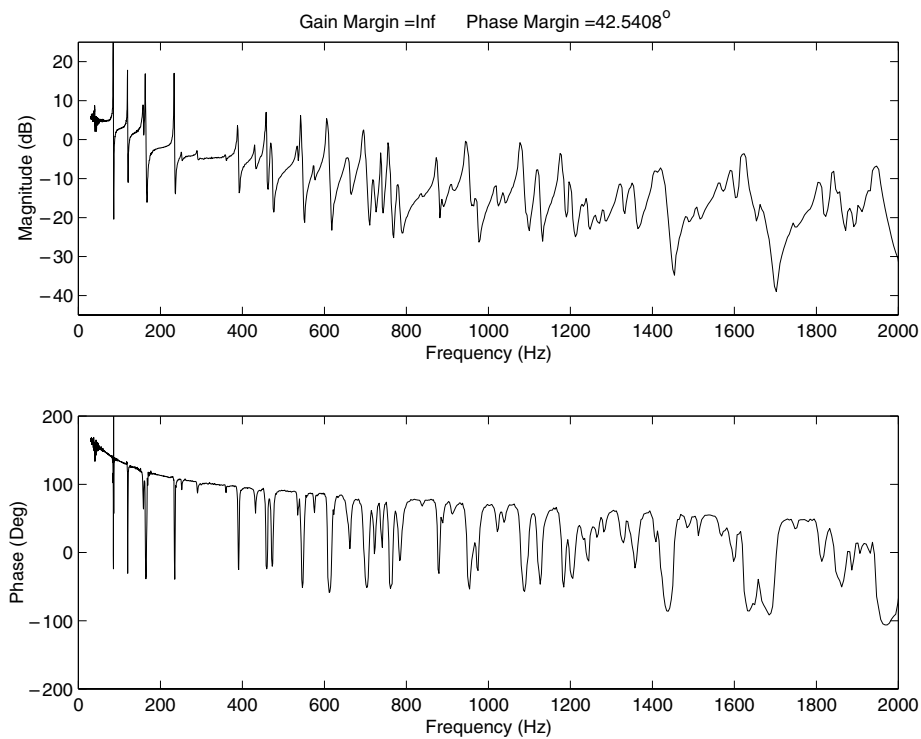


Figure 13. Gain and phase margin of $G_{vv}(j\omega)\tilde{K}(j\omega)$.

and 22.4 dB, respectively. Overall, the experimental and simulated results closely agree, therefore validating the proposed negative capacitance controller.

7. Stability and robustness of the closed loop system

In section 5, the proposed negative capacitance controller is classified as an active shunt. Therefore, stability and robustness issues need to be addressed for the closed

loop system. In this section we will demonstrate that implementation of the proposed negative capacitance controller results in a closed loop system that has good robustness properties.

To determine the gain and phase margin of the closed loop system, the experimental frequency response for the $G_{vv}(j\omega)$ was captured using a Hewlett Packard spectrum analyzer (33120A). The true experimental controller response $\tilde{K}(j\omega)$ is impossible to obtain due to the physical nature of the

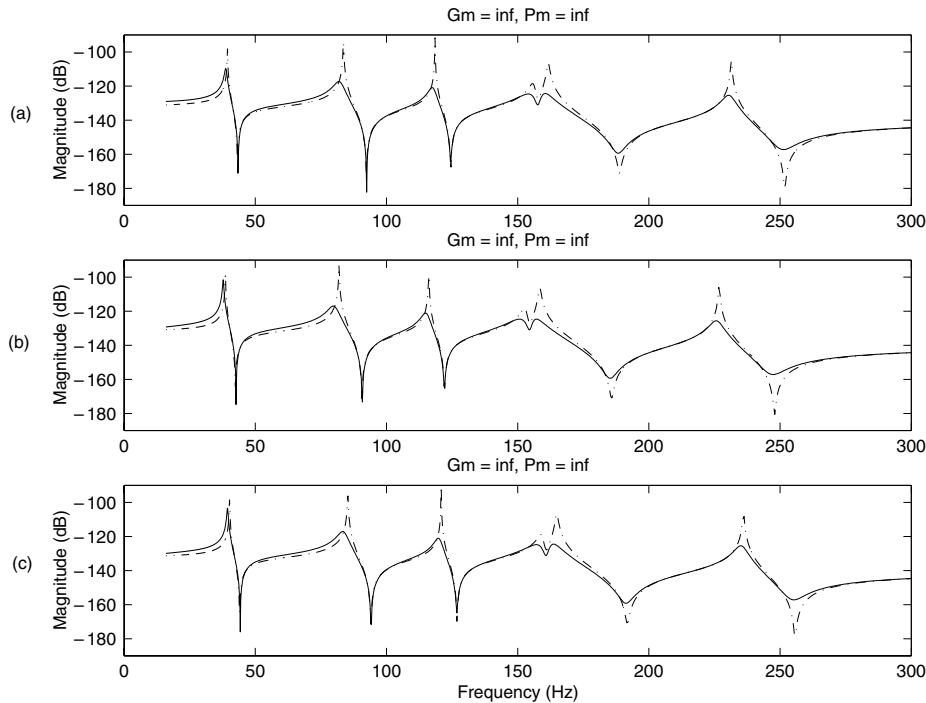


Figure 14. Simulated response: (a) original system, (b) poles moved -2% from the original system, and (c) poles moved $+2\%$ from the original system. $|G_{vv}(0.2, 0.2, s)|$ system ($-\cdot-$) and $|\hat{G}_{vv}(0.2, 0.2, s)|$ system ($—$). Note the simulated gain and phase margin of $G_{vv}(j\omega)\bar{K}(j\omega)$ of subfigure (a)–(c).

piezoelectric layer. Therefore, a simulated controller (36) with appropriate experimental parameters as in table 3, was used to determine the $G_{vv}(j\omega)\bar{K}(j\omega)$. Figure 13 illustrates the magnitude–phase response for $G_{vv}(j\omega)\bar{K}(j\omega)$.

From $G_{vv}(j\omega)\bar{K}(j\omega)$ frequency response, shown in figure 13, the gain and phase margin are found to be ∞ and 42.5408° (at 89.855 Hz) respectively. If the resonance frequencies ω_{mn} of the structure are shifted due to environmental conditions, or perhaps other reasons, the closed loop system will have acceptable robustness.

As an aside, it should be noted that the proposed negative capacitance controller is capable of damping modally dense structures, as shown in figure 12, for the fourth and fifth modes. Also, the control scheme is virtually immune to variations in structural dynamics since it is not tuned into any specific resonance frequency. This is in contrast to previous *passive* shunt networks [9, 10, 16, 17], which are generally sensitive to climatic variations in the resonance frequencies of the underlying structure. This was verified by shifting the simulated resonance frequencies $\pm 2\%$ from the original frequencies. Simulated results shown in figure 14, assuming $Z(s) = \frac{(485 \text{ nF})(80 \Omega)s - 1}{(485 \text{ nF})s}$ for all subfigures, show that the performance of the system is not severely deteriorated by changing resonance frequencies of the base structure. Also, note the appropriate simulated $G_{vv}(j\omega)\bar{K}(j\omega)$ gain and phase margin for each system, as indicated on each subfigure of figure 14.

8. Conclusion

The ‘negative capacitance controller’ has been introduced as an alternative method of reducing structural vibrations, compared

to passive shunt techniques. In the paper we have attempted to clarify that the negative capacitance controller is, in fact, an ‘active shunt’. The effect of the negative capacitance controller was studied theoretically and experimentally on a simply supported plate structure. While achieving comparable performance to passive techniques, the negative capacitance controller is capable of damping multiple modes, requires simple circuitry, is less sensitive to environmental conditions, is relatively robust and is capable of damping modally dense structures, i.e. broadband damping.

Acknowledgments

This research was supported by the Center for Integrated Dynamics and Control (CIDAC) and the Australian Research Council (ARC).

References

- [1] Behrens S 2001 Passive and semi-active vibration control of piezoelectric laminates *Master's Thesis* The University of Newcastle, Australia
- [2] Behrens S, Fleming A J and Moheimani S O R 2001 New method for multiple-mode shunt damping of a structural vibration using a single piezoelectric transducer *Proc. SPIE: Smart Structure and Materials 2001: Damping and Isolation; Proc. SPIE* **4331** 239–50
- [3] Behrens S and Moheimani S O R 2000 Optimal resistive elements for multiple mode shunt damping of a piezoelectric laminate beam *Proc. IEEE Conf. on Decision and Control (Sydney, Australia, Dec. 2000)* pp 4018–23
- [4] Behrens S and Moheimani S O R 2002 Current flowing multiple mode piezoelectric shunt dampener *Proc. SPIE: Smart Structure and Materials: Damping and Isolation (March 2002); Proc. SPIE* **4697** 217–26

- [5] Clephas B 1999 Piezoelectric actuators *Adaptronics and Smart Structures—Basics, Material, Design, and Applications* ed H Janocha (Berlin: Springer) ch 6.2 pp 106–23
- [6] Desoer C A and Kuh E S 1969 *Basic Circuit Theory* (New York: McGraw-Hill)
- [7] Fuller C R, Elliott S J and Nelson P A 1996 *Active Control of Vibration* (New York: Academic)
- [8] Forward R L 1979 Electromechanical transducer-coupled mechanical structure with negative capacitance compensation circuit *US Patent Specification* 4,158,787
- [9] Hagood N W and von Flotow A 1991 Damping of structure vibrations with piezoelectric materials and passive electrical networks *J. Sound Vib.* **14** 243
- [10] Hagood N W and Crawley E F 1991 Experimental investigations of passive enhancement of damping space structures *J. Guid. Control Dyn.* **14** 1100
- [11] Halim D and Moheimani S O R 2000 Optimal placement of a piezoelectric actuator on a thin flexible plate using modal and spatial controllability measures *Technical Report EE9940, School of Electrical Engineering and Computer Science, The University of Newcastle, Australia*
- [12] Horowitz P and Hill W 1980 *The Art of Electronics* 3rd edn (Cambridge: Cambridge University Press)
- [13] Meirovitch L 1996 *Elements of Vibration Analysis* 2nd edn (Sydney: McGraw-Hill)
- [14] Moheimani S O R 2000 Experimental verification of the corrected transfer function of a piezoelectric laminate beam *IEEE Trans. Control Syst. Technol.* **8** 660–6
- [15] Moheimani S O R 2000 Minimizing the effect of out of bandwidth modes in truncated structure models *Trans. ASME, J. Dyn. Syst. Meas. Control* **122** 237–9
- [16] Wu S Y 1996 Piezoelectric shunts with parallel $R-L$ circuit for smart structural damping and vibration control *Proc. SPIE: Smart Structures and Materials: Passive Damping and Isolation (March 1996); Proc. SPIE* **2720** 259–69
- [17] Wu S Y 1998 Method for multiple mode shunt damping of structural vibration using a single PZT transducer *Proc. SPIE: Smart Structure and Materials: Smart Structures and Intelligent System (March 1998); Proc. SPIE* **3327** 159–68
- [18] Wu S Y 2000 Broadband piezoelectric shunts for structural vibration control *Patent Specification* 6,075,309
- [19] Wu S Y 2001 Broadband piezoelectric shunts for passive structural vibration control *Proc. SPIE: Smart Structure and Materials: Smart Structures and Intelligent System (March 2001); Proc. SPIE* **4331** 251–61